Susceptibility and Attenuated Transmissibility of SARS-CoV-2 in Domestic Cats

Linlin Bao[1,2,†], Zhiqi Song[1,2,†], Jing Xue[1,2,†], Hong Gao[1,2,†], Jiangning Liu[1,2,†], Jie Wang[1,2], Qian Guo[2], Binbin Zhao[1,2], Yajin Qu[1,2], Feifei Qi[1,2], Shuran Gong[1,2], Mingya Liu[1,2], Qi Lv[1,2], Dan Li[1,2], Yunlin Han[1,2], Wenjie Zhao[1,2], Shoulong Deng[2], Yunpeng Liu[2], Zhiguang Xiang[2], Bochao Yang[2], Wei Deng[1,2], Haisheng Yu[1,2], Zhe Cong[1,2], Qiang Wei[1,2], Jianguo Xu[4], George F. Gao[3,*], Chuan Qin[1,2,*].

[1]Beijing Key Laboratory for Animal Models of Emerging and Remerging Infectious Diseases, Institute of Laboratory Animal Science, Chinese Academy of Medical Sciences and Comparative Medicine Center, Peking Union Medical College, Beijing, China

[2]NHC Key Laboratory of Human Disease Comparative Medicine, Institute of Laboratory Animal Science, Chinese Academy of Medical Sciences and Comparative Medicine Center, Peking Union Medical College, Beijing, China

[3]Chinese Center for Disease Control and Prevention, Beijing, China

[4]National Institute for Communicable Disease Control and Prevention, Chinese Center for Disease Control and Prevention, Beijing, China

†These authors contributed equally to this work.

*Correspondence should be addressed to Chuan Qin, Email: qinchuan@pumc.edu.cn or George F. Gao, gaof@im.ac.cn.

Abstract

Domestic cats, an important companion animal, can be infected with severe acute respiratory syndrome coronavirus-2 (SARS-CoV-2). This has aroused concern regarding the ability of domestic cats to spread the virus that causes coronavirus disease 2019. We systematically demonstrated the pathogenesis and transmissibility of SARS-CoV-2 in cats. Serial passaging of the virus between cats dramatically attenuated the viral transmissibility, likely owing to variations of the amino acids in the receptor-binding domain sites of angiotensin-converting enzyme 2 between humans and cats. These findings provide insight into the transmissibility of SARS-CoV-2 in cats and provide information for protecting the health of humans and cats.

Article Summary Line: Domestic cats are susceptible to SARS-CoV-2 and have attenuated transmissibility after serial passaging.

Keywords: cats, SARS-CoV-2, COVID-19, transmissibility, pathogenesis, susceptibility

Domestic cats (*Felis domesticus*) are in close contact with humans and have recently gained attention for their susceptibility to severe acute respiratory syndrome coronavirus-2 (SARS-CoV-2). Recent studies demonstrated that experimental cats infected with SARS-CoV-2 via intranasal inoculation could transmit the virus to other cats via respiratory droplets [1, 2] or direct contact [3-5]. The summary of findings in domestic cats to date indicates that cats are highly susceptible to SARS-CoV-2 both in nature and in experimental laboratory settings, and the virus can be spread between cats. Reports suggest that cats can be affected by SARS-CoV-2 via inoculation in a laboratory or exposure to an infected owner. However, the features associated with SARS-CoV-2 infection in domestic cats, the potential risk for cat-to-cat transmissibility of SARS-CoV-2 in nature, and the effectiveness of transmission among cats or of viral spillover into the environment or to pet owners remain unclear. Here, on the basis of the susceptibility and pathogenesis of SARS-CoV-2 in domestic cats, we further evaluated the cat-to-cat transmissibility of SARS-CoV-2 upon serial passaging to provide insight into the potential viral transmissibility between humans and cats.

METHODS

Ethics Statement

Twenty non-neutered felines (ten males and ten females, ranging in age from 8 months to 1.5 years) were evaluated in an animal biosafety level 3 facility. The Institutional Animal Care and Use Committee of the Institute of Laboratory Animal Science (ILAS), Peking Union Medical College (PUMC) (LJN20003) reviewed and authorized all animal procedures.

Study Design

For the animal transmission experiments, 18 outbred cats (nine non-neutered males and nine non-neutered females) were enrolled by one-to-one homosexual cohousing in this serial passage study. Four SARS-CoV-2-infected cats (C0-1 to C0-4; Figure 1) were designated as passage 0 (P_0). Eighteen cats underwent serial passaging via one-to-one homosexual cohousing of a naive cat (recipient) with an infected or exposed cat (donor) for 2 days in a ventilated isolator, in which they had direct contact with each other. To assess transmissibility among the cats after serial passaging, four naive cats (C1-1, C1-2, C1-3, and C1-4) were exposed to P_0 donors (C0-1, C0-2, C0-3, and C0-4) one-on-one at 1 day postinfection (dpi) for 2 days. These cats were designated as passage 1 (P_1). At 3 dpi of P_0, the P_1 cats were separated from the P_0 cats, moved into individual isolators, and cohoused with four naive cats (C2-1, C2-2, C2-3, and C2-4) for 2 days. These cats were designated as passage 2 (P_2). At 5 dpi of P_0, C2-1 and C2-2 were separately introduced to two other naive cats (C3-1 and C3-2) and designated as passage 3 (P_3). To evaluate and compare the transmissibility of SARS-CoV-2 within the same passage but with mixed donors (P_0) from different infectious periods, four P_0 cats were cohoused with another four naive cats (C1-5, C1-6, C1-7, and C1-8, designated as P_4) at 6 dpi of P_0 for 2 days.

Specific antibodies were used to detect SARS-CoV-2 and feline coronavirus (FCoV) before the experiment, and background serum samples were collected from all cats. No serum sample was seropositive by enzyme-linked immunosorbent assay (ELISA) for the spike proteins of either SARS-CoV-2 or FCoV. To observe potential clinical signs, each cat's temperature and weight were recorded daily. To determine the potential viral shedding period of SARS-CoV-2 from cats and evaluate its infectious viral titer, throat and anal swabs

were collected from each cat at 0, 3, 4, 5, 7, 9, 11, 13, and 14 dpi for each passage. Before sample collection, all animals were anesthetized via intramuscular injection with 10 mg/kg tiletamine hydrochloride and zolazepam hydrochloride for injection (Zoletil® 50). At 14 dpi, sera were collected to detect the presence of IgG antibodies that reacted with SARS-CoV-2 antigens. Two cats each from P_0, P_1, P_2, P_3 and P_4 were euthanized and necropsied at 14 dpi or days postexposure (dpe) for histopathological observation.

Viruses and Cells

SARS-CoV-2 (SARS-CoV-2/WH-09/human/2020/CHN/MT093631.2) was isolated by the ILAS, PUMC. Vero E6 cells were prepared to reproduce the SARS-CoV-2 stocks. Cells were incubated at 37°C under 5% CO_2 in Dulbecco's modified Eagle's medium (Invitrogen, Carlsbad, CA, USA) complemented with 10% fetal bovine serum, 100 µg/mL streptomycin, and 100 IU/mL penicillin. SARS-CoV-2 titers were determined via tissue culture infectious dose ($TCID_{50}$) assay.

RT-qPCR

RNA extraction and qRT-PCR were performed as previously reported [6]. Briefly, total RNA was extracted using the RNeasy Mini Kit (Qiagen, Hilden, Germany), and reverse transcription was performed using the PrimerScript RT Reagent Kit (TaKaRa, Japan) following the manufacturer's instructions. qRT-PCR reactions were performed using the PowerUp SYBG Green Master Mix Kit (Applied Biosystems, CA, USA), and samples were processed in duplicate using the following cycling protocol: 50°C for 2 min, 95°C for 2 min, followed by 40

cycles at 95°C for 15 s and 60°C for 30 s, then 95°C for 15 s, 60°C for 1 min, and 95°C for 45 s. The following primer sequences were used for the RT-PCR targeted against the envelope gene of SARS-CoV-2: forward: 5'-TCGTTTCGGAAGAGACAGGT-3', reverse: 5'-GCGCAGTAAGGATGGCTAGT-3'. The PCR products were verified by sequencing using the dideoxy method on an ABI 3730 DNA sequencer (Applied Biosystems). The products were amplified using specific primers during the sequencing; these sequences are available upon request. The sequencing reads obtained were linked using DNAMAN, and the results were compared using the Megalign module in the DNAStar software package (Madison, Wisconsin, USA). A SYBR Green real-time PCR standard curve was generated using serial 10-fold dilutions of a recombinant plasmid with a known copy number (from 1.47×10^{9} to 1.47×10^{1} copies/µL). These dilutions were tested and used as quantification standards to construct a standard curve by plotting the plasmid copy number against the corresponding threshold cycle values. The results are expressed as log10 numbers of genome equivalent copies per mL of sample. The detection limits were ten copy equivalents of RNA per mL of plasma.

ELISA

Sera were collected from the cats at 0, 11, and 14 dpi to measure the SARS-CoV-2 antibody via ELISA. As previously reported [7], 96-well plates were coated with 0.1 µg spike protein of SARS-CoV-2 (Sino Biological, 40591-V08H) overnight at 4°C and blocked with 2% bovine serum albumin/phosphate-buffered saline with Tween 20 (PBST) for 1 h at 37°C temperature. Sera were then diluted at 1:100, added to each well and incubated for 30 min at 37°C, then incubated with horseradish peroxidase (HRP)-labeled goat anti-cat IgG Fc

(Abcam, ab112801) for 30 min at 37°C. The reaction was developed with 3, 3', 5, 5'-Tetramethylbenzidine (TMB) substrate and measured at 450 nm.

Immunohistochemistry and Histopathological Examination

All collected organs and tissues were fixed in 10% buffered formalin solution and used to make paraffin sections (3–4 µm thickness) as per standard protocol. All tissue sections were stained with hematoxylin and eosin (H&E), modified Masson's trichrome, and periodic acid-Schiff (PAS). Histopathological changes were observed under an Olympus microscope (Tokyo, Japan). Slides were examined without knowledge of the animals' identity. For immunohistochemistry (IHC) staining to identify the SARS-CoV-2 antigen, lung tissues sections were stained with 7D2 monoclonal antibody (laboratory preparation [6]) at 4°C overnight, then incubated with HRP-labeled goat anti-mouse IgG (Beijing ZSGB Biotechnology, ZDR-5307) for 1 hour. The sections were then incubated with 3,30-diaminobenzidine tetrahydrochloride (DAB), and the images were viewed under an Olympus microscope.

Confocal Microscopy

To examine the relationship between SARS-CoV-2 and angiotensin-converting enzyme 2 (ACE2), lung tissue sections (3–4 µm) were washed twice with phosphate-buffered saline (PBS), fixed with Immunol Staining Fix Solution (P0098), blocked for 1 h at room temperature with Immunol Staining Blocking Buffer (P0102), and incubated overnight at 4°C with the appropriate primary and secondary antibodies. The nuclei were stained with 4',6-diamidino-

2-phenylindole (DAPI). Anti-SARS-CoV-2 protein (convalescent phase sera of monkey) and anti-ACE2 antibody (rabbit polyclonal antibody, Abcam, ab15348, 1:300) were used as the primary antibodies. The sections were washed with PBS, incubated with secondary antibodies conjugated with fluorescein isothiocyanate (FITC) (goat anti-human, Abcam, ab6854, 1:200) and AF555 (donkey anti-rabbit, Abcam, ab150074, 1:200), and dried at room temperature. Fluorescence was observed via microscopy.

Phylogenetic Analysis of ACE2

The ACE2 protein sequences for the candidate animals and humans were retrieved from GenBank. Multiple-sequence alignment was optimized using MUSCLE (EMBL-EBI, Cambridge, UK). The ACE phylogeny was constructed with MEGA_X_10.1.8 (Philadelphia, Pennsylvania, USA) using the Jones-Taylor-Thornton model and 1000 bootstrap replicates.

Molecular Docking Study

The three-dimensional (3D) structures of the SARS-CoV-2 receptor-binding domain (RBD) and human ACE2 complex (PDB ID: 6M0J) were retrieved from RCSB PDB (https://www.rcsb.org). The initial 3D structures of the SARS-CoV-2 RBD and feline ACE2 complex were modeled by mutating the corresponding residues of human ACE2 in the above-mentioned crystal structure, which included residues 24, 30, 34, 38 and 82, using Schrödinger software (New York, NY, China). The subsequent energy of the side chains of the mutated residues was minimized using Schrödinger until achieving an RMSD convergence threshold of 0.001. The binding affinities (ΔG) of human ACE2, cat ACE2 and

the SARS-CoV-2 RBD were calculated using the molecular mechanics energies combined with the Generalized Born and surface area continuum solvation (MM-GBSA) module, in which the side chains in the RBM of the RBD and the interfacing ACE2 residues (residues 19–85) were allowed to fluctuate flexibly. The other settings were set to the default settings.

Statistical Analysis

Comparisons among groups were determined via two-tailed unpaired Student's t-tests. All data were analyzed with GraphPad Prism 8.0 software (San Diego, CA, USA). $P<0.05$, $P<0.01$, and $P<0.001$ were considered statistically significant.

RESULTS

Clinical Signs, Viral Replication and Pathological Changes of SARS-CoV-2 Infection in Domestic Cats

Six domestic cats (C0-1 to C0-6) were inoculated intranasally with SARS-CoV-2 stock virus at 10^6 50% $TCID_{50}$ (0.4 mL per animal). Following the SARS-CoV-2 challenge, the average body temperature for the six infected cats was approximately 38.5°C (Figure 1A). The infected cats lost <10% body weight (Figure 1A). After the SARS-CoV-2 challenge, the cats exhibited clinical signs including arching of the back and diarrhea which has also been observed in clinical patients. We next determined the viral RNA from throat and anal swabs for 14 days after SARS-CoV-2 infection. Viral RNA from the throat swabs peaked at 3 dpi (average, 5.01 log_{10} RNA copies/mL), then decreased (Figure 1B, left panel). Similarly, viral RNA from the anal swabs peaked at 2.29 log_{10} RNA copies/mL at 7 dpi, then decreased to undetectable

levels at 11 dpi (Figure 1B, right panel).

To identify the histopathological changes in SARS-CoV-2-infected cats, infected cats (C0-5 and C0-6) and two uninfected (control) cats were euthanized and necropsied at 7 dpi. Compared with the lung tissues of the control cats, SARS-CoV-2-infected cats developed moderate interstitial pneumonia accompanied by diffuse alveolar damage associated with SARS-CoV-2 antigen expression, which occurred mainly in the alveolar epithelial cells (Figure 1C). Tissues with thickened alveolar septa were collected for modified Masson's trichrome staining to confirm connective tissue proliferation. Masson staining revealed a small amount of collagen fiber in the thickened alveolar interstitium (Figure 1C). Bronchiolar epithelial cells, some of which were fragmented, showed swelling and degeneration. The affected bronchioles contained large amounts of PAS-positive mucosal substances or PAS-positive denatured and detached bronchiolar epithelium (Figure 1C). Characteristic changes in the lung tissues included thickened and multifocal alveolar septa, mild-to-moderate bronchiolitis with bronchiolar exudate, and many degenerative inflammatory cells, particularly lymphocytes, monocytes, and neutrophils, around the blood vessels. Identification of bronchiolitis in cats has potential implications for SARS-CoV-2 pathogenesis and excretion. Additionally, compared with the control cats, the infected cats showed extra respiratory changes at 7 dpi, including multifocal inflammatory cells consisting of lymphocytes and neutrophils in the intestinal submucosa and muscularis. The splenic lymphoid follicles of the white pulp and the germinal centers of the lymph nodes exhibited multifocal lymphocyte depletion (Figure 1D).

Cat-to-Cat Transmissibility of SARS-CoV-2 via Serial Passaging in Cohoused Cats

To explore the relative risk of SARS-CoV-2 transmissibility among cats via close contact, four serial passage experiments via one-to-one homosexual cohousing were carried out according to the schedule in Figure 2A. For the P_1 cats, viral RNA from throat swabs exhibited shorter shedding periods (3–11 dpe) and lower peaks (5−7 dpe) than those of P_0 (average for $10^{2.71}$ RNA copies/mL, Supplementary Figure 1A). Viral RNA from P_1 anal swabs was only detected at 5 dpe (Supplementary Figure 2A). The viral RNA peaks from the throat and anal swabs of P_1 were significantly lower than those of P_0 (Figure 2B). Viral shedding durations from the throat swabs did not significantly differ between P_0 and P_1 (median: 11 versus 9 days); however, the viral shedding durations from the anal swabs of P_1 were significantly shorter than those of P_0 (median: 1 versus 3 days; Figure 2B). For the P_2 and P_3 cats, no viral shedding was detected from the throat or anal swabs (Figure 2B). Compared with that of P_1, the peak and duration of the viral shedding from the throat swabs of P_2 (median: 0 versus 9 days) and the duration from the anal swabs of P_2 were significantly decreased (median: 0 versus 1 day). No significant difference occurred in the viral shedding peak from the anal swabs of P_2 (Figure 2B). For P_4, the viral shedding peak and duration from the throat and anal swabs were significantly decreased compared with those of P_0 (Figure 2B).

P_1 and P_4 were further compared to evaluate the SARS-CoV-2 transmissibility within the same passage but with different infectious periods of the donors (P_0). The peak (mean: 3.43 versus 1.23 $\log_{10}$ RNA copies/mL) and duration (median: 9 versus 0 days) of the viral shedding from the throat swabs differed significantly between P_1 and P_4, but the peak (mean: 1.21 versus 1.03 $\log_{10}$ RNA copies/ml) and duration (median: 1 versus 0 days) of the

viral shedding from the anal swabs did not (Figure 2B). For all tested cats, the detectable viral RNA was greater, and the shedding duration was longer from the throat swabs than from the anal swabs. These data suggest that the viral shedding peak and duration decreased significantly after serial passaging of SARS-CoV-2 in cats, and no viral RNA was detected from P_2. The SARS-CoV-2 transmissibility was also weakened in the later stages of infection.

Specific antibodies were tested to confirm whether individuals in each passage were infected with SARS-CoV-2. P_0 and P_1 cats that were seronegative prior to the experiments were seropositive at 11 and 14 dpe. The specific antibody titers differed significantly between P_0 and P_1 at 11 and 14 dpi (Figure 2C). The specific antibody titers from P_2, P_3, and P_4 were below the detection limits.

At 14 dpi and dpe, two cats each from P_0, P_1, P_2, P_3 and P_4 were euthanized for histopathological observation. Compared with P_0 at 14 dpi, only P_1 developed SARS-CoV-2-related moderate interstitial pneumonia accompanied by mild-to-moderate thickened alveolar interstitium (Figure 2D, left panel). In P_1, modified Masson's trichrome staining revealed a small amount of collagen fiber in the thickened alveolar interstitium (Figure 2D, left panel). Bronchiolar epithelial cells, some of which were fragmented, showed swelling and degeneration, and the affected bronchioles contained a few PAS-positive mucosal substances and denatured/detached bronchiolar epithelium (Figure 2D, right panel). No substantial changes occurred in the lungs of the P_2, P_3 or P_4 cats (Figure 2D, left panel). The bronchioles of the P_1 cats contained some mucosal substances, but these were minimal in P_2, P_3 and P_4 (Figure 2D, right panel).

Colocalization and Interaction of SARS-CoV-2 with the ACE2 Receptor in the Feline Lungs and Intestines

To elucidate the mechanism of SARS-CoV-2 infection and decreased transmissibility in domestic cats, we investigated the interaction of feline ACE2 and SARS-CoV-2. Lung and intestinal sections from two infected cats (C0-1 and C0-2) at 14 dpi were double-stained with antibodies against SARS-CoV-2 and ACE2. Viral antigens were distributed in the lungs and intestines (Figure 3). SARS-CoV-2 expression in the intestines likely explains the diarrhea in these cats and is consistent with this clinical manifestation in some patients with COVID-19. Additionally, SARS-CoV-2-postive cells were co-located with ACE2 in the cytoplasm, suggesting that feline ACE2 is the receptor for SARS-CoV-2.

Next, we performed a phylogenetic analysis of ACE2, the receptor for SARS-CoV-2, from a range of candidate animals (Figure 4A). The ACE2 proteins of SARS-CoV-2-susceptible species, including humans, monkeys, and Syrian hamsters (another subcluster), were clustered together. Cats from this study fell within another cluster closer to the subcluster of ferrets and dogs. Alignment of ACE2 from humans, SARS-CoV-2-susceptible animals (rhesus macaques) [7-9], Syrian hamsters [10, 11], SARS-CoV-2-nonsusceptible animals (mice [6] and pigs [1, 12]) and domestic cats [13] suggested that feline ACE2 was highly similar to human ACE2, with five variations at the interface (Figure 4B). Using molecular modeling, we analyzed the differences in binding modes and binding affinities between SARS-CoV-2 RBDs, particularly the receptor-binding motif (RBM) and human ACE2 and feline ACE2. ACE2 receptors from both genera exhibited similar binding interaction networks towards the SARS-CoV-2 RBD (Figure 4C, Supplementary Tables 1 and 2), indicating the susceptibility of cats to SARS-CoV-2. We then compared the interactions between the RBD

and the five amino acid residues in the human and cat ACE2 receptors. Among them, two residues had identical interactions with the RBD: Asp30/Glu30 and Met82/Thr82 in the human ACE2/feline ACE2. However, at amino acids 24 and 34 of the ACE2 receptors, Gln24 and His34 of the human ACE2 receptors formed a hydrogen bond and Van der Waals interactions with Asn487 and Tyr453, whereas Leu24 and Tyr34 of feline ACE2 had fewer interactions with the RBD. At position 38, Glu38 of the feline ACE2 formed hydrogen bonds with Tyr449 and Gln498 of the RBD, while Asp38 of the human ACE2 interacted only with Tyr449 (Figure 4D). The Δ*G* of the feline ACE2 combined with the viral RBD was −101.643 Kcal/mol, which was slightly weaker than that of human ACE2 (−107.516 Kcal/mol). This might be contributed to the lower transmissibility of SARS-CoV-2 among cats, but further studies are required to determine the effects of the variations associated with the lower transmissibility.

DISCUSSION

Previous studies suggested that cats were infected with SARS-CoV-2 from patients with COVID-19; however, no direct evidence exists that infected cats can spread SARS-CoV-2 to humans. Here, we report that experimental cats can be infected with SARS-CoV-2 via intranasal inoculation without mortality. Consistent with our results, other studies have reported that cats are highly suspectable to SARS-CoV-2 infection via intranasal and oral routes with prolonged periods of throat viral shedding and clinicopathological abnormalities, but they are unlikely to develop the clinical disease [1, 2, 14]. As reported, the main histopathology of SARS-CoV-2-infected lungs of human patients with COVID-19 includes exudate and hemorrhaging, diffuse alveolar damage, macrophage infiltration, hyaline

membrane formation, and multinucleated syncytial cells with atypical enlarged pneumocytes [15]. The pathophysiological patterns of COVID-19 are related to its duration in different individuals [16]. Similar to the results of Gaudreault et al., who found mild-to-moderate neutrophilic and lymphocytic tracheobronchoadenitis with related detection of viral RNA and viral antigens [14], we found that the pathological changes in the lungs of primary infected cats showed mild-to-moderate bronchiolitis with exudate in the bronchioles, thickened alveolar septa, diffuse alveolar damage, focal hemorrhaging, and occasional multinucleated syncytial cells. Particularly, cats infected with SARS-CoV-2 develop tracheobronchitis, necrosis, inflammation of the tracheobronchial glands, and diffuse alveolar damage [17, 18]. Additionally, SARS-CoV-2 was expressed in the intestines of the infected cats, similar to the observations of Shi et al., who found the virus in the intestines of many animals. This is also consistent with the clinical sign of patients with COVID-19 [1].

Consistent with previous reports, the cats transmitted SARS-CoV-2 via close contact. However, the SARS-CoV-2 transmissibility and pathogenicity were significantly reduced by sequential passaging within the cats, which ruled out interference due to gender differences because we used equal numbers of male and female cats in this study. The reduced and limited transmissibility and pathogenic ability after passaging revealed that cats might be transiently infected by SARS-CoV-2 in nature. Additionally, viral sequencing of all P_1 animals in the first stage of the experiment enabled determining whether changes in viral sequencing might be involved in the attenuation, but no SARS-CoV-2 sequence changes were found in the P_1 cats. No viral sequencing was performed for the P_2, P_3 or P_4 animals because we could not isolate the virus from these cats. Braun et al. found that SARS-CoV-2 consensus sequences remain largely unchanged within cats; these authors speculated that a

narrow transmission bottleneck of SARS-CoV-2 occurs in domestic cats [19]. Recent genomic analysis comparing human ACE2 with ACE2 from 410 species of vertebrates revealed that ~40% of the species are potentially vulnerable to SARS-CoV-2 infection [20]. In this study, phylogenetic analysis of ACE2 revealed that cats were in the medium category for SARS-CoV-2 infection. Our results suggest that compared with human ACE2 [21], five variations exist at the binding sites of the feline ACE2 receptor. In contrast to a recent study confirming a 3–4-fold weaker binding affinity of feline ACE2 with the SARS-CoV-2 RBD [22], the mutated amino acids at sites 24 and 34 of the feline ACE2 receptor reduce the binding affinity of the receptor to the SARS-CoV-2 RBD, which may explain why cat-to-cat transmissibility of SARS-CoV-2 is reduced over time in contrast to the sustained human-to-human transmission [23].

ACKNOWLEDGMENTS

We thank National Mega Projects of China for Major Infectious Diseases (2017ZX10304402), CAMS Initiative for Innovative Medicine of China (2016-I2M-2-006) and the National Key Research and Development Project of China (2020YFA0707803) for their support of the animal model study.

COMPETING INTERESTS

The authors have no competing interests to declare.

AUTHOR CONTRIBUTIONS

Conceptualization: C.Q.; Methodology: L.B., Z.S., Jing Xue, Hong Gao, J.L.; Investigation: L.B., Z.S., Jing Xue, Hong Gao, J.L., J.W., Qian Guo, B.Z., Y.Q., F.Q., S.G., M.L., Q.L., D.L., Y.H., W.Z., S.D., Y.L., Z.X., B.Y., W.D., H.Y., Z.C., Q.W., Jianguo Xu, G.G. and C.Q.; Writing – Original Draft: Jing Xue and Z.S.; Writing – Review and Editing: G.G. and C.Q.; Funding Acquisition: C.Q.; Resources: C.Q.; Supervision: C.Q.

FIGURE LEGENDS

Figure 1. SARS-CoV-2 pathogenesis in domestic cats. A, Clinical signs in each domestic cat. Changes in body temperature and body weight in the cats were recorded at the indicated time points prior to SARS-CoV-2 challenge. B, Viral replication from throat and anal swabs. SARS-CoV-2 RNA was detected via RT-qPCR from swabs from six infected cats at the indicated time points. The red solid lines represent the average of all animals at the indicated time points. C, Histopathological changes and immunohistochemical (IHC) examination of the lungs of SARS-CoV-2-infected cats. Lung tissues from infected cats (C0-5 and C0-6) were collected at 7 dpi and stained with hematoxylin and eosin (H&E). SARS-CoV-2 antigens were detected with anti-spike antibody 7D2 via IHC examination. Compared with the normal controls, modified Masson's trichrome staining revealed few collagen fibers (blue-stained fibers) in the thickened alveolar interstitium of the lungs of infected cats. Histopathological changes and periodic acid-Schiff (PAS) staining of the bronchioles of SARS-CoV-2-infected cats. D, Extrarespiratory histopathological changes in the SARS-CoV-2-infected cats. Lesions were found in the intestines, spleen and lymph nodes via H&E staining. The larger box shows the smaller box in greater detail. The right panel shows the boxed area in the left panel. Black scale bar = 100 µm, red scale bar = 50 µm. All data represent three independent experiments.

Figure 2. Cat-to-cat transmission of SARS-CoV-2 via serial passaging in cohoused cats. A, Experimental design for SARS-CoV-2 transmission among cats. N=4 per single passage in P_0, P_1, P_2, and P_4, N=2 in P_3. FCoV-specific antibody was tested from serum from each cat prior to the study. IN, intranasal inoculation. B, Comparison of viral shedding from throat swabs

and anal swabs. The peak (left panel) and duration (right panel) of viral shedding in throat and anal swabs were compared among different passages (P_0, P_1, P_2 and P_3) or the same passage but on a different day from the primary donor postinoculation (P_1 and P_4). C, Levels of binding antibody against SARS-CoV-2. SARS-CoV-2 spike-1-specific antibodies from different passage groups were examined and compared at 0, 11 and 14 dpe. All data are presented as the means ± SD from three independent experiments. Statistical analysis was performed via two-tailed unpaired Student's t-tests, *P<0.05, **P<0.01, ***P<0.001. ns, not significant. D, Histopathological analysis of the lungs and bronchioles from different passage groups. Two cats from P_0, P_1, P_2, P_3 and P_4 were euthanized at 14 dpe for histopathological observation. Histopathological changes via H&E and modified Masson's trichrome staining in the lungs of cats after serial passaging are shown in the left panels. Histopathological changes shown via H&E and PAS staining in the bronchioles from sequential sections of cats after serial passaging are shown in the right panels. The larger box shows the smaller box in greater detail. Black scale bar = 100 μm, red scale bar = 50 μm. All data represent three independent experiments.

Figure 3. Colocalization of the cat ACE2 receptor with SARS-CoV-2. Two infected cats from P_0 were euthanized at 14 dpi. SARS-CoV-2 (green) and feline ACE2 (red) were localized in the lungs (A) and intestines (B). The SARS-CoV-2 antigen and feline ACE2 receptor are shown colocalized in yellow. The nuclei were stained with DAPI (blue). The larger box shows the smaller box in greater detail. Sections from two uninfected cats were used as negative controls. Data are representatives of three independent experiments.

Figure 4. Comparisons of interactions at the human ACE2-SARS-CoV-2 RBD and feline ACE2-SARS-CoV-2 interfaces. A, Phylogenetic tree of the ACE2 proteins of humans and 15 representative animals. Humans, rhesus macaques and Syrian hamsters, susceptible to SARS-CoV-2 are highlighted in orange. Cats tested in the present study are highlighted in purple. Mice and pigs (not susceptible to SARS-CoV-2) are highlighted in gray. B, Multiple alignment of the amino acid residues from ACE2 proteins of the highlighted animal species. The amino acid residues binding with the RBD between the human and animal ACE2 are in yellow and blue. C, Interaction model of the SARS-CoV-2 RBD (blue) and human ACE2 (orange) or feline ACE2 (purple). Compared with human ACE2, five amino acid residues from feline ACE2 are indicated, and the SARS-CoV-2 receptor-binding motif (RBM) is shown in red. The lower panels are magnifications of the upper panels. D, Comparison of the binding force and length of five amino acid positions at the human ACE2-SARS-CoV-2 RBD and feline ACE2-SARS-CoV-2 RBD interfaces.

References

1. Shi J, Wen Z, Zhong G, et al. Susceptibility of ferrets, cats, dogs, and other domesticated animals to SARS-coronavirus 2. Science (New York, NY) **2020**; 368:1016-20.
2. Bosco-Lauth AM, Hartwig AE, Porter SM, et al. Experimental infection of domestic dogs and cats with SARS-CoV-2: Pathogenesis, transmission, and response to reexposure in cats. Proceedings of the National Academy of Sciences of the United States of America **2020**; 117:26382-8.
3. Halfmann PJ, Hatta M, Chiba S, et al. Transmission of SARS-CoV-2 in Domestic Cats. The New England journal of medicine **2020**; 383:592-4.
4. Segalés J, Puig M, Rodon J, et al. Detection of SARS-CoV-2 in a cat owned by a COVID-19-affected patient in Spain. Proceedings of the National Academy of Sciences of the United States of America **2020**; 117:24790-3.
5. Barrs VR, Peiris M, Tam KWS, et al. SARS-CoV-2 in Quarantined Domestic Cats from COVID-19 Households or Close Contacts, Hong Kong, China. Emerging infectious diseases **2020**; 26.
6. Bao L, Deng W, Huang B, et al. The pathogenicity of SARS-CoV-2 in hACE2 transgenic mice. Nature **2020**.
7. Deng W, Bao L, Liu J, et al. Primary exposure to SARS-CoV-2 protects against reinfection in rhesus macaques. Science (New York, NY) **2020**.
8. Chandrashekar A, Liu J, Martinot AJ, et al. SARS-CoV-2 infection protects against rechallenge in rhesus macaques. Science (New York, NY) **2020**.
9. Yu P, Qi F, Xu Y, et al. Age-related rhesus macaque models of COVID-19. Animal models and experimental medicine **2020**; 3:93-7.
10. Boudewijns R, Thibaut HJ, Kaptein SJF, et al. STAT2 signaling restricts viral dissemination but drives severe pneumonia in SARS-CoV-2 infected hamsters. Nature communications **2020**; 11:5838.
11. Chan JF, Zhang AJ, Yuan S, et al. Simulation of the Clinical and Pathological Manifestations of Coronavirus Disease 2019 (COVID-19) in a Golden Syrian Hamster Model: Implications for Disease Pathogenesis and Transmissibility. Clinical infectious diseases : an official publication of the Infectious Diseases Society of America **2020**; 71:2428-46.
12. Schlottau K, Rissmann M, Graaf A, et al. SARS-CoV-2 in fruit bats, ferrets, pigs, and chickens: an experimental transmission study. The Lancet Microbe **2020**.
13. Chiocchetti R, Galiazzo G, Fracassi F, Giancola F, Pietra M. ACE2 Expression in the Cat and the Tiger Gastrointestinal Tracts. Frontiers in veterinary science **2020**; 7:514.
14. Gaudreault NN, Trujillo JD, Carossino M, et al. SARS-CoV-2 infection, disease and transmission in domestic cats. Emerging microbes & infections **2020**; 9:2322-32.
15. Huang C, Wang Y, Li X, et al. Clinical features of patients infected with 2019 novel coronavirus in Wuhan, China. Lancet (London, England) **2020**; 395:497-506.
16. Camporota L, Vasques F, Sanderson B, Barrett NA, Gattinoni L. Identification of pathophysiological patterns for triage and respiratory support in COVID-19. The Lancet Respiratory medicine **2020**; 8:752-4.
17. Martina BE, Haagmans BL, Kuiken T, et al. Virology: SARS virus infection of cats and ferrets. Nature **2003**; 425:915.
18. Ng SK. Possible role of an animal vector in the SARS outbreak at Amoy Gardens. Lancet (London, England) **2003**; 362:570-2.
19. Braun KM, Moreno GK, Halfmann PJ, et al. Transmission of SARS-CoV-2 in domestic cats imposes a narrow bottleneck. bioRxiv : the preprint server for biology **2020**.
20. Damas J, Hughes GM, Keough KC, et al. Broad host range of SARS-CoV-2 predicted by comparative and structural analysis of ACE2 in vertebrates. Proceedings of the National Academy of Sciences of the United States of America **2020**; 117:22311-22.
21. Lu R, Zhao X, Li J, et al. Genomic characterisation and epidemiology of 2019 novel coronavirus: implications for virus origins and receptor binding. Lancet (London, England) **2020**.
22. Wu L, Chen Q, Liu K, et al. Broad host range of SARS-CoV-2 and the molecular basis for SARS-CoV-2 binding to cat ACE2. Cell discovery **2020**; 6:68.
23. Li Q, Guan X, Wu P, et al. Early Transmission Dynamics in Wuhan, China, of Novel Coronavirus-Infected Pneumonia. N Engl J Med **2020**:10.1056/NEJMoa2001316.

Figure 1

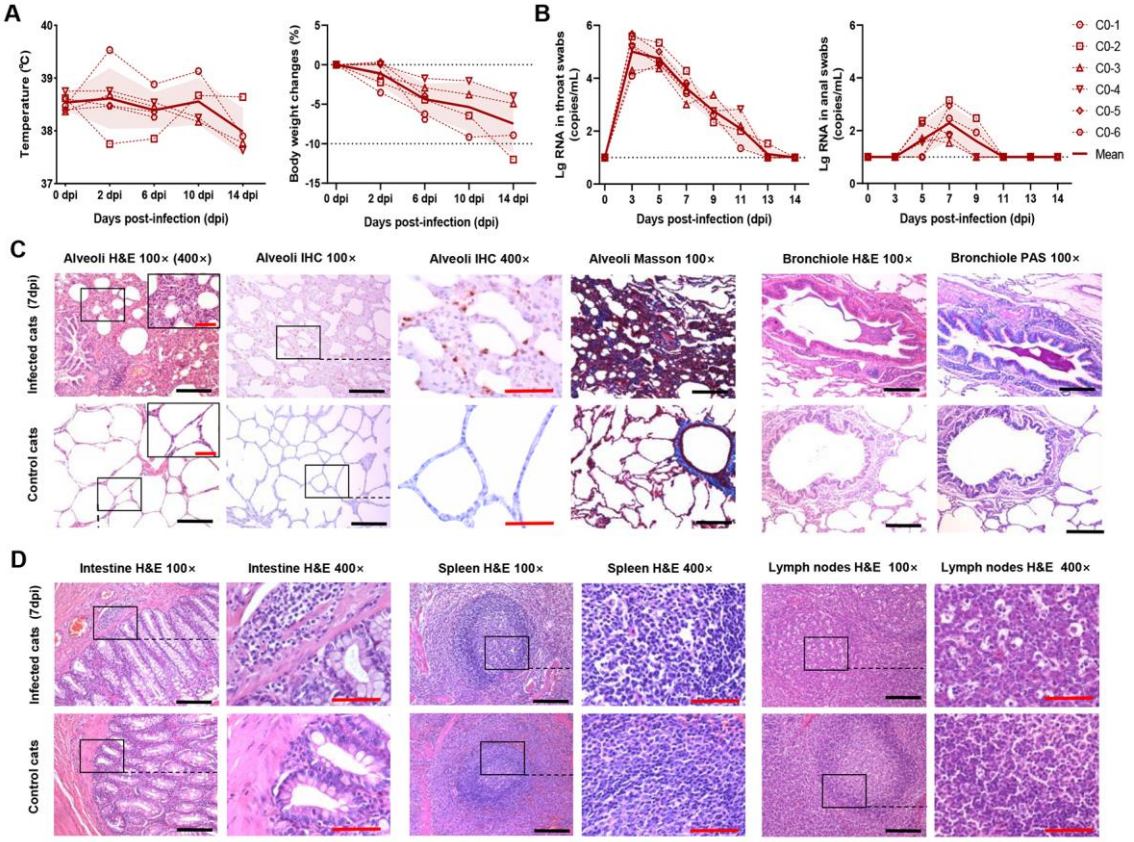
A
Temperature (℃)
Days post-infection (dpi)
Body weight changes (%)
Days post-infection (dpi)
B
Lg RNA in throat swabs (copies/mL)
Days post-infection (dpi)
Lg RNA in anal swabs (copies/mL)
Days post-infection (dpi)
C0-1
C0-2
C0-3
C0-4
C0-5
C0-6
Mean
C
Alveoli H&E 100× (400×)
Alveoli IHC 100×
Alveoli IHC 400×
Alveoli Masson 100×
Bronchiole H&E 100×
Bronchiole PAS 100×
Infected cats (7dpi)
Control cats
D
Intestine H&E 100×
Intestine H&E 400×
Spleen H&E 100×
Spleen H&E 400×
Lymph nodes H&E 100×
Lymph nodes H&E 400×
Infected cats (7dpi)
Control cats

Figure 2

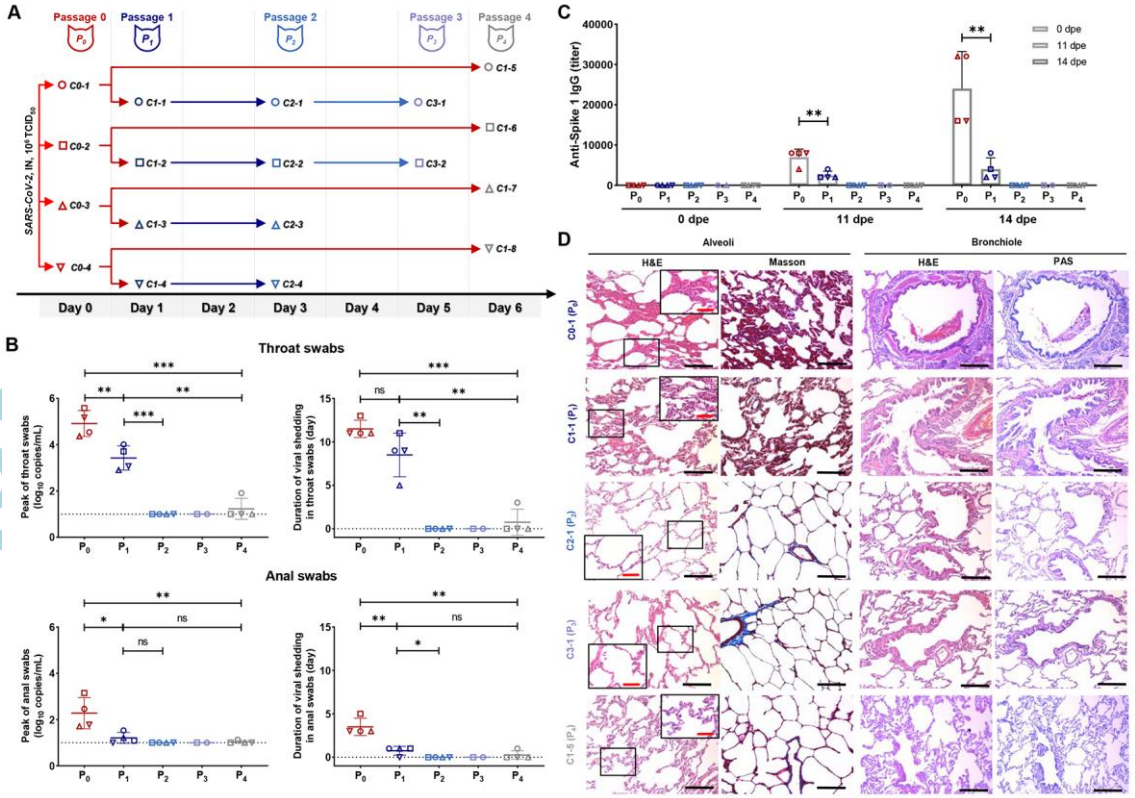

Figure 3

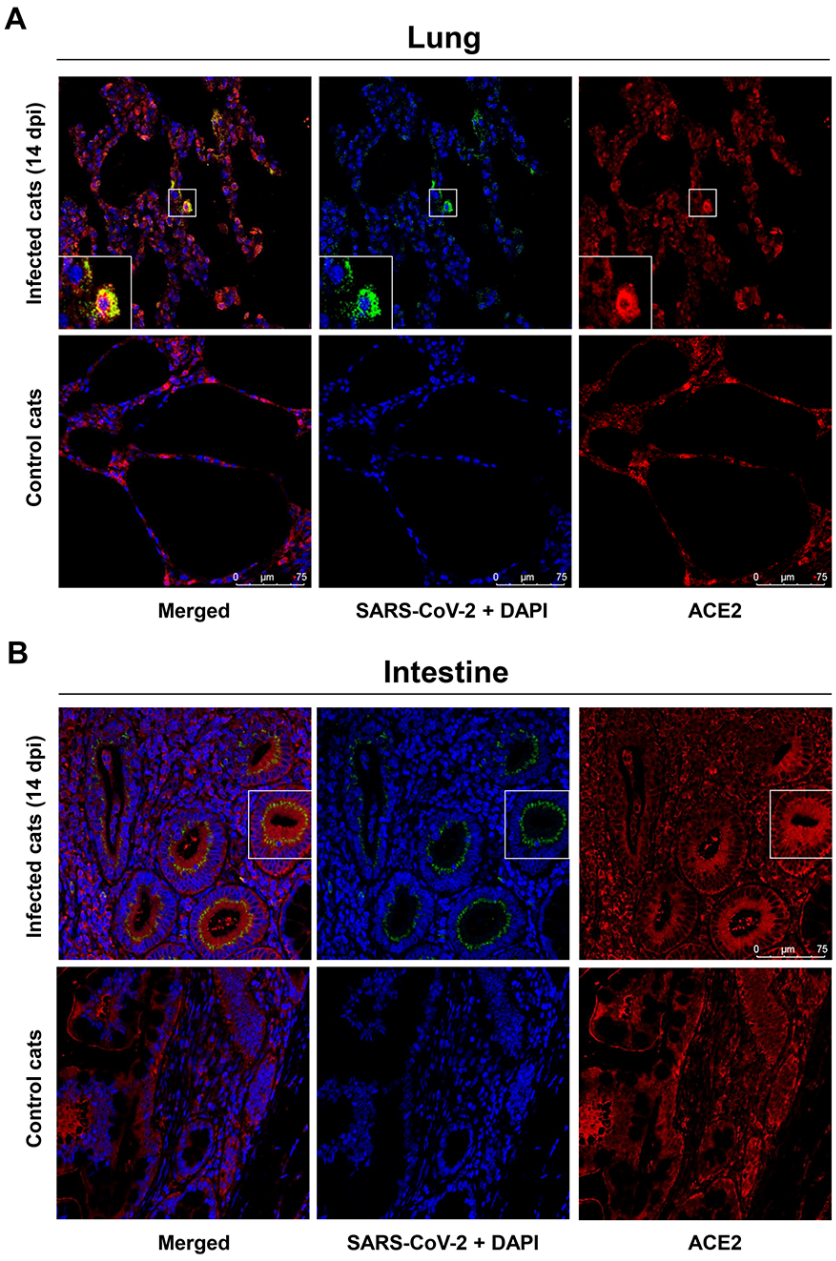
A
Lung
Infected cats (14 dpi)
Control cats
Merged
SARS-CoV-2 + DAPI
ACE2
B
Intestine
Infected cats (14 dpi)
Control cats
Merged
SARS-CoV-2 + DAPI
ACE2

Figure 4

A

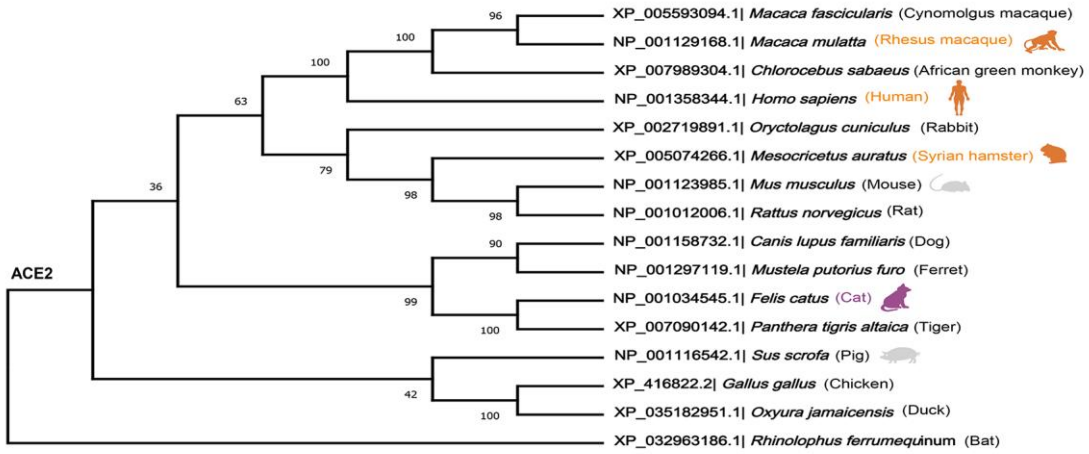

B

ACE2 amino acid	24	27	28	30	31	34	35	37	38	41	42	79	82	83	330	353	354	355	357	393
Human *(Homo sapiens)*	Q	T	F	D	K	H	E	E	D	Y	Q	L	M	Y	N	K	G	D	R	R
Rhesus macaque *(Macaca mulatta)*	Q	T	F	D	K	H	E	E	D	Y	Q	L	M	Y	N	K	G	D	R	R
Syrian hamster *(Mesocricetus auratus)*	Q	T	F	D	K	Q	E	E	D	Y	Q	L	N	Y	N	K	G	D	R	R
Domestic cat *(Felis catus)*	L	T	F	E	K	Y	E	E	E	Y	Q	L	T	Y	N	K	G	D	R	R
Mouse *(Mus musculus)*	N	T	F	N	N	Q	E	E	D	Y	Q	T	S	F	N	H	G	D	R	R
Pig *(Sus scrofa)*	L	T	F	E	K	L	E	E	D	Y	Q	I	T	Y	N	K	G	D	R	R
consensus in all species		*	*				*	*		*	*				*		*	*	*	*
consensus in sensitive species		*	*		*		*	*		*	*	*		*	*	*	*	*	*	*
distinct site in cat vs human	*			*		*			*				*							

C

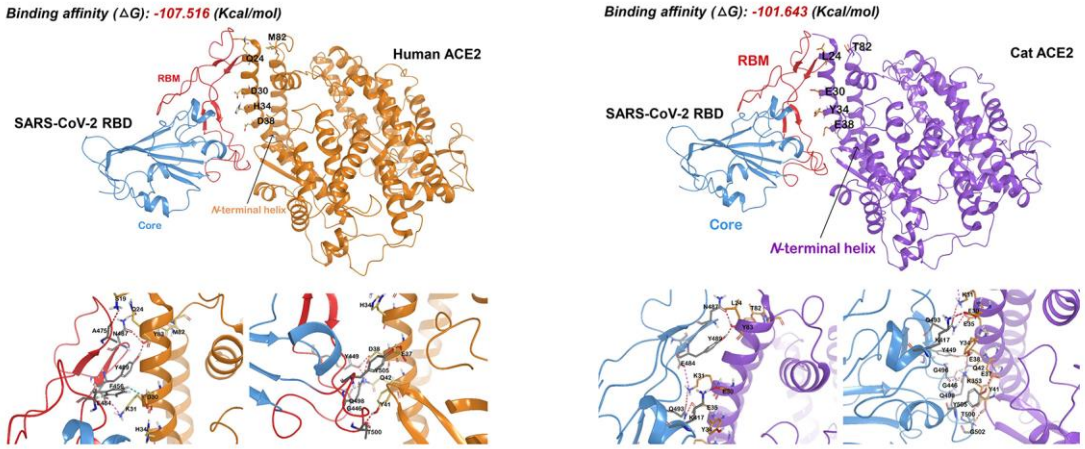

D

ACE2 amino acid position	Human ACE2	Length (Å)	Binding force	SARS-CoV-2 RBD	Binding force	Length (Å)	Cat ACE2
24	Q	2.7	Hydrogen bond	N487	/	/	L
30	D	2.9	Hydrogen bond/Salt bridge	K417	Hydrogen bond/Salt bridge	2.8	E
34	H	2.9	Van der Waals force	Y453	/	/	Y
38	D	2.7, /	Hydrogen bond	Y449, Q498	Hydrogen bond	2.6, 3.0	E
82	M	3.6	Van der Waals force (weak)	F486	Van der Waals force (weak)	3.3	T